MI Preprint Series

Mathematics for Industry
Kyushu University

Gyroscopic Analogy of Coriolis Effect of Rotating Stratified Flows Confined in a Spheroid

Yuki Miyachi
& Yasuhide Fukumoto

MI 2017-1

(Received January 18, 2017)

Institute of Mathematics for Industry
Graduate School of Mathematics
Kyushu University
Fukuoka, JAPAN

Gyroscopic Analogy of Coriolis Effect of Rotating Stratified Flows Confined in a Spheroid

Yuki Miyachi[1]

[1]Graduate School of Mathematics, Kyushu University, 744 Motooka, Nishi-ku, Fukuoka 819-0395, Japan

E-mail: y-miyachi@math.kyushu-u.ac.jp

Yasuhide Fukumoto

Institute of Mathematics for Industry, Kyushu University, 744 Motooka, Nishi-ku, Fukuoka 819-0395, Japan

E-mail: yasuhide@imi.kyushu-u.ac.jp

Abstract. An insight is gained into the mechanism of system rotation for suppressing the Rayleigh-Taylor instability (RTI) by drawing analogy with the gyroscopic effect. A rotating flow of a stratified fluid confined in a spheroid, subject to gravity force, whose velocity field is linear in coordinates, is equivalent, in the Boussinesq approximation, to the motion of the Lagrange top, a heavy symmetrical rigid body. The sleeping top corresponds to the state in which a heavy fluid lies on top of a lighter fluid. Specifically, we investigate the incompressible two-layer RTI confined in the lower-half of a spheroid rotating about the axis of symmetry oriented parallel to the vertical direction. We derive the dispersion relation and the critical rotation rate for suppressing the axisymmetric mode of RTI. The gyroscopic analogy accounts for decrease of the critical rotation rate with oblateness of the spheroid. The stabilizing effect of rotation is enhanced for the half spheroid as compared with a circular cylinder of finite length.

Keywords: rotating Rayleigh-Taylor instability, Coriolis force, gyroscopic force, baroclinic fluid, Lagrange top, internal inertia-gravity wave, spheroidal container

1. Introduction

In the investigation of the Rayleigh-Taylor instability (RTI) in a rotating frame, Chandrasekhar [1] claimed that "it follows that in the present case rotation does not affect the instability or stability, as such, of a stratification". In the field of the atmospheric and oceanic fluid dynamics, this problem has not attract much attention, possibly because less concern in unstably stratified fluid. However, the dispersion relation of the internal inertia-gravity waves for a continuously stratified incompressible fluid suggests that the rotation competes with the gravitational instability and its

stabilizing effect is able even to overcome the gravitational instability of an unstably stratified fluid. Incidentally, we are reminded of the Richardson-number criterion that the flow with sufficiently strong shear destabilizes the stably stratified configuration [2, 3, 4].

Introduce the Cartesian coordinates (x, y, z), with the gravity force, of acceleration g, directed in the negative z-axis. In the Boussinesq approximation, we partition the density of the fluid into the reference constant value ρ_0 and the deviation ρ' as $\rho = \rho_0 + \rho'(x, y, z, t)$, with t the time, and denote the Brunt-Väisälä frequency to be $N^2 = -(g/\rho_0)(\partial\rho'/\partial z)$. When N is constant, the frequency ω of the internal inertia-gravity wave, with the horizontal wavenumbers k and l and the vertical wavenumber m is given by

$$\omega^2 = \frac{m^2}{k^2 + l^2 + m^2} f^2 + \frac{k^2 + l^2}{k^2 + l^2 + m^2} N^2, \tag{1}$$

where $f = 2\Omega_0$ is the Coriolis parameter, with Ω_0 being the angular velocity of the system rotation as a whole [5, 6, 7]. The dispersion relation (1) reveals competition between the stabilizing action of the Coriolis force, featured by f^2, and the destabilizing action of the gravity force, featured by N^2 in case $N^2 < 0$. For a horizontally long wave ($k^2 + l^2 \ll m^2$) being required for a complete suppression, the approximate form of the dispersion relation (1) becomes

$$\omega^2 \approx f^2 + \frac{k^2 + l^2}{m^2} N^2. \tag{2}$$

This is an analog of the dispersion relation for the Poincaré wave, the surface gravity wave of shallow water in a rotation frame [6]. The dispersion relation (1) and (2) indicates that the instability with long horizontal wavelength can be suppressed by the rotation if the rotation rate is sufficiently large, that is, if $f^2 m^2 > -N^2(k^2 + l^2)$. This is genuinely a three-dimensional phenomenon in the sense both the horizontal and the vertical wavenumbers take part in.

Recently the suppression of RTI by rotation was addressed in a confined geometry. For a rotating two-layer flow confined in a circular cylinder of finite extent, with the axis of rotation perpendicular to the interface between the layers, the critical rotation rate for the stability was deduced and was compared with the experimental results [8]. Possibility of complete suppression of RTI was further explored [9]. They overtured a scenario for stabilization by rotation as a competition between the two-dimensionalization of the Taylor-Proudman theorem and destabilization by baroclinically generated vorticity. The waves with wavelength longer than a critical wavelength are stabilized by rotation while this is not the case with the shorter one [9]. Carnevale *et al.* [10] analyzed numerically the rotating RTI under the Boussinesq approximation for negative, but small in magnitude, values of the Atwood number $A = (\rho_2 - \rho_1)/(\rho_2 + \rho_1)(< 0)$. Here ρ_1 and ρ_2 are the mass densities of the upper and the lower layers. They attributed the stabilizing mechanism to the Coriolis force acting on the vortex rings generated at an early stage of RTI. They claimed that the

rotation can suppress RTI over the whole wavelength range. The elimination of the short-wavelength RTI may be the cut-off due to the viscosity. Tao *et al.* [11] considered theoretically whether the rotation can suppress or not RTI at arbitrary Atwood numbers in a rotating system where the the acceleration is provided solely by the centrifugal force of the two uniform inviscid fluids and found that rotation acts to diminish the growth rate. They reckoned the Coriolis force as a restoring force acting on the perturbed interface.

In this investigation, we illustrate the rotational suppression of a two-layer RTI confined in the lower half of a spheroidal container, by referring to the analogy that holds between the rotating stratified flow in a spheroid and the motion of the Lagrange top, a heavy symmetrical top, subject to the gravity force, with the center of the gravity and a fixed point on the axis of symmetry [12]. The configuration where a heavy fluid layer lies on a light one under rotation is likened to the sleeping top state, and the Coriolis force is likened to the gyroscopic term. The parabolic deformation of the density interface is precisely incorporated [13, 9]. In particular, we illuminate the effect of the bottom topography, by varying the aspect ratio from prolate to oblate spheroids, and compare it with the case of flat bottom.

Analogies between stratified incompressible flows under the gravitational force and motion of a heavy rigid body are traced back to the eighteenth century. Greenhill [14] noticed that the Euler equation for motion of a free rigid body describes flows, with a class of spacially linear velocity fields, of an ideal incompressible homogeneous fluid inside an ellipsoid. Poincaré [15] studied the motion of the incompressible fluid confined in a spheroid which rotates about its axis of symmetry accompanied by the precession. The analogy is helpful for understanding the phenomena of the baroclinic as well as the barotropic rotating flows [6, 16]. The thermally stratified inviscid incompressible fluid, with linear-in-coordinates velocity fields, confined in an ellipsoidal cavity, is shown to be equivalent to a dynamical system called the *baroclinic top* [17]. As a common feature, the motion of a rigid body obeys the Hamiltonian system, endowed with the Lie-Poisson structure [12, 23].

Dolzhansky [12, 17] extensively investigated the baroclinic top equations in the quasi-geostrophic and thermal-wind approximation, and gave an interpretation of the mechanism for generation of atmospheric cyclogenesis due to the conversion of available potential energy into the kinetic energy associated with the vertical vorticity. This pertains to the baroclinic instability [6, 16]. He also applied the gyroscopic analogy to treat the general circulation of the atmosphere, supplemented by a linear friction, for simulating the effect of the planetary boundary layer and of the Newtonian heat sources, stemming from temperature deviations from the background, though the treatment is limited to an asymmetric top. Furthermore, for a spherically symmetric top, the comparison was made between the analytical solutions of the quasi-geostrophic three-wave model and of the top equations [18] in order to understand the mechanism for the suppression of the gravity waves in the quasi-geostrophic approximation (see also [19, 20]). Holm [21] extended the model to include the effect of salinity gradients with the

spatially linear profiles. He developed a systematic method of using the tensor-moment dynamics with an advantage of explicitly incorporating the boundary condition. So far gyroscopic analogies have extensively been invoked for stably stratified flows, but not much for unstably stratified flows. This paper highlights the gyroscopic effect possessed by the Coriolis force and its ability to surpass the gravitational instability.

In section 2, we revisit the analogy showing that the sleeping top corresponds to an unstably stratified state. We point out the correspondence between the Coriolis and the gyroscopic forces. In section 3, we model the two-layer rotating flow confined in the lower half part of a spheroid with the symmetric axis parallel to the vertical direction. The interface shape is precisely incorporated and an approximate form of the dispersion relation is presented for small angular velocity of the system rotation and for the near critical state, by means of the variational formulation developed by Scase *et al.* [9]. The critical rotation rate for stability is calculated, with emphasis put on its shape dependence of the container, the oblateness of the spheroid or a circular cylinder. The gyroscopic analogy helps to account for the variation of the critical rotation rate with the aspect ratio of the spheroid. The last section (section 4) is devoted to a summary and conclusions.

2. Analogy between rotating stratified flow in spheroid and Lagrange top

We start with a brief outline of the analogy of a rotating flow in the spheroid with the motion of the Lagrange top [12].

2.1. Derivation of baroclinic top equations

Consider a flow of an inviscid incompressible stratified fluid confined in an upright spheroidal container with its boundary prescribed by

$$S := \frac{x^2 + y^2}{a_1^2} + \frac{z^2}{a_3^2} - 1 = 0. \tag{3}$$

We assume that the principal axis coincide with the coordinate axes, with the two of principle axes, lying on the horizontal plane, equal in length $a_1 = a_2$ (Figure 1).

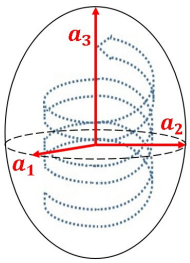

Figure 1. A sketch of the rotating flows (dotted helical wide arrow) confined in a vertically placed spheroidal container, of length a_1, a_2 ($a_1 = a_2$) and a_3, with the symmetric axis oriented in the vertical direction.

We denote the density by $\rho = \rho_0 + \rho'(x, y, z, t)$, the buoyancy by $b' = -g\rho'/\rho_0$. The vorticity $\boldsymbol{\Omega} = \nabla \times \boldsymbol{v}$, with $\boldsymbol{v}$ being the velocity field, and $\boldsymbol{q} = \nabla\rho'/\rho_0$ are governed, in the Boussinesq approximation, by

$$\frac{\partial \boldsymbol{\Omega}}{\partial t} - (\boldsymbol{\Omega}\cdot\nabla)\boldsymbol{v} + (\boldsymbol{v}\cdot\nabla)\boldsymbol{\Omega} \quad = \boldsymbol{q}\times\boldsymbol{g}, \tag{4}$$

$$\frac{\partial \boldsymbol{q}}{\partial t} + (\boldsymbol{v}\cdot\nabla)\boldsymbol{q} = -\sum_{k=1}^{3} q_k \nabla v_k, \tag{5}$$

where $\boldsymbol{g} = -g\boldsymbol{e}_z$. The right-hand side of (4) represents the baroclinic torque term. As is read from (4), the baroclinic torque, which acts when the density gradient is not parallel to the gravity, creates and intensifies the vorticity. This is the source for the baroclinic instability in the atmospheric and oceanic fluid dynamics [6, 16].

Introduce the solenoidal vector fields, being linear in coordinates, which are particular stationary solutions of (4) and (5),

$$\boldsymbol{W}_1 = -\frac{a_2}{a_3} z\boldsymbol{j} + \frac{a_3}{a_2} y\boldsymbol{k}, \quad \boldsymbol{W}_2 = -\frac{a_3}{a_1} x\boldsymbol{k} + \frac{a_1}{a_3} z\boldsymbol{i}, \quad \boldsymbol{W}_3 = -\frac{a_1}{a_2} y\boldsymbol{i} + \frac{a_2}{a_1} x\boldsymbol{j},$$

where $\boldsymbol{i}, \boldsymbol{j}$ and $\boldsymbol{k}$ are the unit basis vectors of the reference coordinate frame (x, y, z). The axial symmetry ($a_1 = a_2$) should be kept in view. We seek a general non-stationary solution of (4) and (5) in the form

$$\boldsymbol{v}(\boldsymbol{x}, t) = \sum_{k=1}^{3} \omega_k(t)\boldsymbol{W}_k(\boldsymbol{x}). \tag{6}$$

where $\boldsymbol{x} = (x, y, z)$. The coefficients $\omega_k(t)(k = 1, 2, 3)$, being functions of t, are called the Poincaré parameters [12]. Substitution from (6), (4) and (5) are reduced to

$$\dot{\boldsymbol{m}} = \boldsymbol{\omega}\times\boldsymbol{m} + g\boldsymbol{\sigma}\times\boldsymbol{l}_0, \tag{7}$$

$$\dot{\boldsymbol{\sigma}} \ = \boldsymbol{\omega}\times\boldsymbol{\sigma}, \tag{8}$$

where $\boldsymbol{m} = I\boldsymbol{\omega}$, $\omega_k = (a_1a_2a_3/a_kI_k)\Omega_k$, without taking summation in k. Here I is the inertia-moment tensor, being a diagonal matrix, as defined by

$$I = \begin{pmatrix} I_1 & 0 & 0 \\ 0 & I_2 & 0 \\ 0 & 0 & I_3 \end{pmatrix} = \begin{pmatrix} a_2^2 + a_3^2 & 0 & 0 \\ 0 & a_3^2 + a_1^2 & 0 \\ 0 & 0 & a_1^2 + a_2^2 \end{pmatrix}. \tag{9}$$

The components of the vector $\boldsymbol{\sigma}$ measure the density difference along the principal axes of the ellipsoid defined by

$$\boldsymbol{\sigma} = \frac{1}{\rho_0}\left(a_1 \frac{\partial\rho'}{\partial x}\bigg|_0 \boldsymbol{i} + a_2 \frac{\partial\rho'}{\partial y}\bigg|_0 \boldsymbol{j} + a_3 \frac{\partial\rho'}{\partial z}\bigg|_0 \boldsymbol{k}\right). \tag{10}$$

In (4), $\boldsymbol{l}_0$ is a constant vector defined by $\boldsymbol{l}_0 = a_1\cos\alpha_1\boldsymbol{i} + a_2\cos\alpha_2\boldsymbol{j} + a_3\cos\alpha_3\boldsymbol{k}$ where $\alpha_i(i = 1, 2, 3)$ is the angle between the principal axis x, y and z and the gravity acceleration vector $\boldsymbol{g}$. This system of (7) and (8) is nothing but the Lie-Poisson equation

for the heavy symmetrical top with a fixed point along the symmetry axis, viewed in terms of the coordinate frame tied to the body. In this context, $\boldsymbol{m}$ is the angular momentum, $\boldsymbol{\omega}$ is the angular velocity, $\boldsymbol{\sigma}$ is the gravity-direction vector and $\boldsymbol{l}_0$ is a constant vector in the body frame. The gyroscopic terms stem from the first terms on the right-hand side of (7) and (8). The last term of (7) originates from the baroclinic torque.

By exploiting the analogy with the sleeping top, we unravel the stabilization mechanism of the RTI which occurs at the rotating angular velocity larger than a critical value [8, 9, 10, 22]. This scenario is illustrated in the following section.

2.2. Sleeping top and its counterpart

We recall the stability result of the sleeping state of the Lagrange top governed by (7) and (8). The sleeping top is a steady solution

$$\omega_1 = \omega_2 = 0, \qquad \sigma_1 = \sigma_2 = 0, \qquad \omega_3 = \omega_{30}, \qquad \sigma_3 = \sigma_{30}, \tag{11}$$

and $\boldsymbol{l} = (0, 0, -a_3)$ for the upright orientation of the symmetric axis. Here the variables marked by the index 0 are at our disposal. The well-known condition for the stability of the sleeping top reads

$$\omega_{30}^2 > \frac{4\sigma_{30} g a_3 I_1}{I_3^2}, \tag{12}$$

where σ_{30} corresponds to the mass of the top, a_3 to the length from the fixed point to the center of the gravity [23].

The translation of this result into the rotating stratified flow in the spheroid is straightforward. By definition, ω_3 is constant multiple of the vertical vorticity Ω_3 and $\omega_1 = \omega_2 = 0$ means that there is no vertical flow, with the horizontal circulatory-flow velocity being independent of z. In view of (10), σ_3 is a density gradient in the vertical direction multiplied by a_3/ρ_0. For $\sigma_3 > 0$, the vertical density gradient $\partial\rho'/\partial z > 0$, corresponding to the state of a circulatory flow of a stratified fluid in which a lighter fluid can sustain a heavier fluid. This analogy provides a clue for understanding the ability of a light fluid layer to lift heavier ones above it. The suppression of RTI by rotation as a whole is reasoned in an analogous manner [8, 9, 10, 22].

It is noteworthy that the gyroscopic force is indispensable for the stabilization of the sleeping top. The motion of the Lagrange top is mathematically equivalent to that of a spherical pendulum with charge, subject to the magnetic field generated by the magnetic monopole sitting at the fixed point [24]. When the magnetic field is switched off, the pendulum exhibits precessional motion, but is unable to stay above the fixed point. It is the Lorenz force acting on the pendulum that can maintain the pendulum above the fixed point. By invoking the analogy, the Coriolis force is indispensable for lifting the heavy fluid layer above a light fluid layer. With this analogy kept in our mind, we tackle with the problem of stabilization of RTI by rotation for a two-layer flow confined in a spheroid.

3. Rayleigh-Taylor instability in a half spheroid

We adopt the two-layer rotating flow in a circular cylinder [9] to that confined in the lower half of a spheroidal container as shown in Figure 2. For simplicity, we assume that the fluids are confined below a rigid lid placed on the equatorial plane. The upper (lower) layer is denoted by subscript 1 (2). We use cylindrical polar coordinates (r, θ, z) with unit vectors $\boldsymbol{e}_r$, $\boldsymbol{e}_\theta$ and $\boldsymbol{e}_z$ along the radial, the azimuthal and the vertical directions respectively.

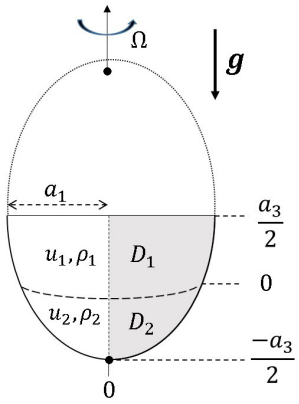

Figure 2. Two-layer fluids, subject to the gravity force with acceleration g, confined in the lower half of a spheroid with the length of the symmetric axis a_3 and the rest a_1, rotating with the angular velocity $\boldsymbol{\Omega}$ along z-axis. The region is divided into two parts $D_1(D_2)$ corresponding to the upper (lower) layer. A rigid lid is placed at $z = a_3/2$. The interface $z = z_0(r)$ is described by the dashed parabolic line.

3.1. Equations and boundary conditions

We introduce the coordinate system rotating, with angular velocity $\boldsymbol{\Omega} = \Omega \boldsymbol{e}_z$, to identify a stationary solution easily. The half length of the symmetric axis is a_3 and that of the other principal axes is a_1. Ignoring viscosity, we write the momentum equation for the fluid in each layer as

$$\frac{D\boldsymbol{u}_j}{Dt} + 2\boldsymbol{\Omega} \times \boldsymbol{u}_j + \boldsymbol{\Omega} \times (\boldsymbol{\Omega} \times \boldsymbol{x}) = -\frac{1}{\rho_j} \nabla p_j - g\boldsymbol{e}_z \quad (j = 1, 2), \tag{13}$$

where $\boldsymbol{x}$ is the position vectors in the rotating frame and $\boldsymbol{u}_j$ is the velocity field of the layer j. The first term on the left-hand side of (13) is the Lagrange derivative of the velocity, the second is the Coriolis force and the third is the centrifugal force.

When the fluid system execute the rigid-body rotation, $\boldsymbol{u}_j = 0$ is a steady solution and the corresponding pressure distribution is

$$p_j = p_0 - \rho_j \left\{ gz - \frac{\Omega^2}{2} \left(r^2 - \frac{5}{8} a_1^2 \right) \right\}, \tag{14}$$

with some constant p_0. We set the vertical coordinate z so that, in the absence of rotation ($\boldsymbol{\Omega} = \mathbf{0}$), the density interface coincides with $z = 0$. The stress or the pressure should be continuous across the interface. By requiring $p_1 = p_2$ on the interface $z = z_0(r)$, we obtain the form of the interface as

$$z_0(r) = \frac{\Omega^2}{2g}\left(r^2 - \frac{5}{8}a_1^2\right). \tag{15}$$

Note that the interface is a isobaric surface and that its height is independent of the fluid density ρ_1 and ρ_2, although its stability may be altered by the density profile.

For later use, we define the radius a of the intersection of the interface with the spheroidal wall from the center, obtained as the simultaneous solution of (3) and (15) for $r = \sqrt{x^2 + y^2}$, giving

$$a^2 = \frac{1}{2a_1^2\Omega^4}\left(a_1^4\Omega^4 - 4a_3^2g^2 + \sqrt{8g^2a_3^2\left(2a_3^2g^2 + a_1^4\Omega^4\right)}\right). \tag{16}$$

For small values of $|\Omega|$, (16) is approximated by

$$a^2 \approx \frac{3}{4}\left(1 + \frac{a_1^2\Omega^2}{12ga_3}\right)a_1^2. \tag{17}$$

The amplitude of the perturbation of the velocity and the pressure, superposed on the hydrostatic state is assumed to be small. Suppose that the density interface is perturbed as

$$z = z_0(r) + \epsilon\zeta(r, \theta, t), \tag{18}$$

where $\epsilon|\zeta| \ll a_3$. We describe the velocity and the pressure perturbations in terms of scalar potentials ϕ_1 and ϕ_2 in such a way that (13) is automatically satisfied to $\mathcal{O}(\epsilon)$ [25].

$$\boldsymbol{u}_j = \epsilon\left\{\left(1 + \frac{1}{4\Omega^2}\right)\frac{\partial^2}{\partial t^2}\nabla\phi_j - \frac{1}{2\Omega}\frac{\partial}{\partial t}(\boldsymbol{e}_z \times \nabla\phi_j) + \boldsymbol{e}_z \times (\boldsymbol{e}_z \times \nabla\phi_j)\right\}, \tag{19}$$

$$p_j = p_0 - \rho_j g\left\{z - z_0(r)\right\} - \epsilon\rho_j\left\{\frac{\partial\phi_j}{\partial t} + \frac{1}{4\Omega^2}\frac{\partial^3\phi_j}{\partial t^3}\right\}, \tag{20}$$

for $j = 1, 2$. Imposition of the incompressibility condition $\nabla \cdot \boldsymbol{u}_j = 0$ brings in equation governing $\phi_j (j = 1, 2)$.

$$\{\partial_t^2\nabla^2 + 4\Omega^2\partial_z^2\}\phi_j = 0 \quad (j = 1, 2). \tag{21}$$

being the equation for the inertia-gravity waves [5, 7]. We seek the solution of (21) complying with the conditions of no penetrating flow through the spheroidal wall

$$\boldsymbol{u} \cdot \boldsymbol{n} = 0, \tag{22}$$

where $\boldsymbol{n}$ is the unit outward normal vector to the spheroidal surface. The velocity should be non-singular on the axis of rotation ($r = 0$).

$$r\frac{\partial \phi_j^2}{\partial r} \to 0 \text{ as } r \to 0. \tag{23}$$

At the interface $z = z_0(r) + \epsilon\zeta$, we require continuity of the pressure and of the normal velocity

$$p_1 = p_2, \tag{24}$$

$$\frac{D}{Dt}(z_0(r) + \epsilon\zeta) = \boldsymbol{u} \cdot \boldsymbol{e}_z. \tag{25}$$

We seek the normal-mode solutions of the form

$$\phi = \hat{\phi}(r, z)\exp\{i(\omega t + m\theta)\},\ \ \zeta = \hat{\zeta}(r)\exp\{i(\omega t + m\theta)\}, \tag{26}$$

where $m \in \mathbb{N} \cup \{0\}$ is the azimuthal wavenumber. Substitution of (26) into (21) yields

$$\frac{1}{r}\frac{\partial}{\partial r}\left(r\frac{\partial \hat{\phi}_j}{\partial r}\right) - \frac{m^2}{r^2}\hat{\phi}_j + (1-\mu^2)\frac{\partial^2 \hat{\phi}_j}{\partial z^2} = 0, \tag{27}$$

where $\mu = 2\Omega/\omega$ [26]. The boundary condition (23) and (22) read, respectively,

$$r\frac{\partial \hat{\phi}_j^2}{\partial r} \to 0 \text{ as } r \to 0, \tag{28}$$

$$\left(r\frac{\partial \hat{\phi}_j}{\partial r} + m\mu\hat{\phi}_j\right)a_3^2 = -(\mu^2-1)a_1^2 z\frac{\partial \hat{\phi}_j}{\partial z} \quad \text{at} \quad S = 0, \tag{29}$$

where the definition (3) for the spheroidal surface is to be remembered. The condition (24) of pressure continuity across the interface $z = z_0(r)$ yields, at order ϵ,

$$i\omega\mu^2\hat{\zeta} = \frac{2\Omega^2}{g}\left(1 - \frac{1}{\mu^2}\right)\left(\frac{1+A}{A}\hat{\phi}_2 - \frac{1-A}{A}\hat{\phi}_1\right). \tag{30}$$

The kinematic condition (25) is specialized, at $\mathcal{O}(\epsilon)$, to, on either side of the interface,

$$i\omega\mu^2\hat{\zeta} = z_0'\left(\frac{\partial \hat{\phi}_j}{\partial r} + \frac{\mu m}{r}\hat{\phi}_j\right) - (1-\mu^2)\frac{\partial \hat{\phi}_j}{\partial z} \quad (j = 1, 2), \tag{31}$$

where $z_0' \equiv dz_0/dr$.

3.2. Variational formulation

Following the ingenious treatment of the preceding investigation [9], we appeal to the variational formulation for manipulating the dispersion relation. The variational principle has an advantage of gaining the eigenvalue with a high accuracy, without having to use the accurate eigenfunction. The variational functional $\Phi[\hat{\phi}_1, \hat{\phi}_2]$ is

constructed by multiplying (27) by $\rho_j\hat{\phi}_j$ and integrating over the domain $D = D_1 \cup D_2$ (see Figure 2).

$$\Phi = \frac{1}{2\pi}\int_D \rho\hat{\phi}\left\{\frac{1}{r}\frac{\partial}{\partial r}\left(r\frac{\partial\hat{\phi}}{\partial r}\right) - \frac{m^2}{r^2}\hat{\phi} + (1-\mu^2)\frac{\partial^2\hat{\phi}}{\partial z^2}\right\} dV. \tag{32}$$

Following the method outlined in [26], we rewrite the integral (32) in conservative form

$$\begin{aligned}\Phi = &\int_{\hat{D}} \rho\left\{\frac{1}{r}\frac{\partial}{\partial r}\left(r\hat{\phi}\frac{\partial\hat{\phi}}{\partial r}\right) + (1-\mu^2)\frac{\partial}{\partial z}\left(\hat{\phi}\frac{\partial\hat{\phi}}{\partial z}\right)\right\} dA\\ &- \int_{\hat{D}} \rho\left\{\left(\frac{\partial\hat{\phi}}{\partial r}\right)^2 + \frac{m^2}{r^2}\hat{\phi}^2 + (1-\mu^2)\left(\frac{\partial\hat{\phi}}{\partial z}\right)\right\} dA,\end{aligned} \tag{33}$$

where integration is implemented over the domain $\hat{D}$ in the meridional plane given by $\hat{D} = \{(r,z) \mid 0 \le r < a_1, -a_3(1-r^2/a_1^2)^{1/2} \le z < 0\}$.

We evaluate the first integration over D_1 and D_2 separately. Defining I_1 to be the integral over D_1, we have

$$\begin{aligned}I_1 = &\int_{z_0(0)}^{z_0(a)}\int_0^{r_0(z)} \frac{\rho_1}{r}\frac{\partial}{\partial r}\left(r\hat{\phi}_1\frac{\partial\hat{\phi}_1}{\partial r}\right) rdrdz + \int_{z_0(a)}^{a_3/2}\int_0^{R(z)} \frac{\rho_1}{r}\frac{\partial}{\partial r}\left(r\hat{\phi}_1\frac{\partial\hat{\phi}_1}{\partial r}\right) rdrdz\\ &+ \int_0^a\int_{z_0(r)}^{a_3/2} \rho_1(1-\mu^2)\frac{\partial}{\partial z}\left(\hat{\phi}_1\frac{\partial\hat{\phi}_1}{\partial z}\right) rdzdr + \int_a^{a_1}\int_{-Z(r)}^{a_3/2} \rho_1(1-\mu^2)\frac{\partial}{\partial z}\left(\hat{\phi}_1\frac{\partial\hat{\phi}_1}{\partial z}\right) rdzdr,\end{aligned} \tag{34}$$

where $r_0(z)$ is the inverse of $z_0(r)$, and $R(z) = a_1(1-(z+a_3/2)^2/a_3^2)^{1/2}$ and $Z(r)+a_3/2 = a_3(1-r^2/a_1^2)^{1/2}$ represent the container wall. The definition of a is given by (17). By virtue of the boundary conditions, (34) becomes, upon integration,

$$\begin{aligned}I_1 = &\rho_1\int_0^a \hat{\phi}_1\left\{z_0'\frac{\partial\hat{\phi}_1}{\partial r} - (1-\mu^2)\frac{\partial\hat{\phi}_1}{\partial z}\right\}\Big|_{z=z_0(r)} rdr - \rho_1\mu m\int_{z_0(a)}^{a_3/2}\hat{\phi}_1^2\Big|_{r=R(z)} dz\\ &+ \rho_1(1-\mu^2)\frac{a_1^2}{a_3^2}\int_{z_0(a)}^{a_3/2} z\hat{\phi}_1\left.\frac{\partial\hat{\phi}_1}{\partial z}\right|_{r=R(z)} dz - \rho_1\frac{a_3^2}{a_1^2}\int_a^{a_1}\frac{1}{z}\hat{\phi}_1\left(r\frac{\partial\hat{\phi}_1}{\partial r} + \mu m\hat{\phi}_1\right)\Big|_{z=-Z(r)} rdr.\end{aligned} \tag{35}$$

Here the first term has been obtained by applying the change of integration variable to $\rho_1\int_{z_0(0)}^{z_0(a)} r\hat{\phi}_1\frac{\partial\hat{\phi}_1}{\partial r}|_{r=r_0(z)}dz$. Repeating the similar procedure, we reduce the second integral of (33) to

$$\begin{aligned}I_2 = &-\rho_2\int_0^a \hat{\phi}_2\left\{z_0'\frac{\partial\hat{\phi}_2}{\partial r} - (1-\mu^2)\frac{\partial\hat{\phi}_2}{\partial z}\right\}\Big|_{z=z_0(r)} rdr - \rho_2\mu m\int_{a_3/2}^{z_0(a)}\hat{\phi}_2^2\Big|_{r=R(z)} dz\\ &+ \rho_2(1-\mu^2)\frac{a_1^2}{a_3^2}\int_{a_3/2}^{z_0(a)} z\hat{\phi}_2\left.\frac{\partial\hat{\phi}_2}{\partial z}\right|_{r=R(z)} dz + \rho_2\frac{a_3^2}{a_1^2}\int_0^a\frac{\hat{\phi}_2}{z}\left(r\frac{\partial\hat{\phi}_2}{\partial r} + \mu m\hat{\phi}_2\right)\Big|_{z=-Z(r)} rdr.\end{aligned} \tag{36}$$

If $\hat{\phi}$ is an exact solution of (27), $\Phi(\hat{\phi}) = 0$. It follows from (33) that

$$\int_D \rho \left\{ \left(\frac{\partial \hat{\phi}}{\partial r} \right)^2 + \frac{m^2}{r^2} \hat{\phi}^2 + (1-\mu^2) \left(\frac{\partial \hat{\phi}}{\partial z} \right) \right\} dA = -I_1 - I_2, \tag{37}$$

because of construction of (32).

Here the reduced form (35) and (36) should be substituted for I_1 and I_2 in (37), and the resulting expression is used for the second integral of (33). A further simplification of (35) and (36) is achieved by exploiting the equation obtainable from (30) and (31) by eliminating ζ.

$$z_0' \frac{\partial \hat{\phi}_j}{\partial r} - (1-\mu^2) \frac{\partial \hat{\phi}_j}{\partial z} = -z_0' \frac{\mu m}{r} \hat{\phi}_j + \frac{2\Omega^2}{g} \left(1 - \frac{1}{\mu^2} \right) \left(\frac{1+A}{A} \hat{\phi}_2 - \frac{1-A}{A} \hat{\phi}_1 \right) \tag{38}$$

on the either side ($j = 1, 2$) of the interface $z = z_0(r)$. After simplification with this help, we eventually arrived at

$$\Phi = \frac{(\rho_2 - \rho_1)(1-\mu^2)}{4g} \int_0^a \left\{ \omega^2 \left[\frac{1+A}{A} \hat{\phi}_2 - \frac{1-A}{A} \hat{\phi}_1 \right]^2 \right.$$
$$\left. + \left[\left(\frac{g z_0'}{\Omega^2 r} \right) \frac{\Omega^2}{1-\mu^2} \left(r \frac{\partial}{\partial r} + 2\mu m \right) - g \frac{\partial}{\partial z} \right] \left[\frac{1+A}{A} \hat{\phi}_2^2 - \frac{1-A}{A} \hat{\phi}_1^2 \right] \right\} \Big|_{z=z_0(r)} r dr. \tag{39}$$

Many terms have been canceled with each other by virtue of (38), and there remains to impose the boundary conditions at the interface.

Following [9], we build the functions $\hat{\phi}_1$ and $\hat{\phi}_2$, together with the eigenvalue ω, by superposing the eigenfunctions of (27), that attains the extremum of Φ.

$$\hat{\phi}_{jn}(r, z) = J_m \left(\frac{k_n r}{a} \right) \cosh \left(\frac{k_n}{a} \frac{\left[z \mp \frac{a_3}{2} \right]}{\sqrt{1-\mu^2}} \right), \tag{40}$$

with $n = 1, 2, \ldots$. Here J_m is a Bessel function of the first kind, k_n is to be specialized below We take the minus or plus sign in (40) according to whether $j = 1$ or 2 respectively. The trial solution (40) satisfies both (27) and the no penetrating-flow condition at $r = 0$ and $z = \pm a_3/2$. The radial no penetrating condition at $z = a_3/2$ and $r = a_1$ reads, in view of (29),

$$\frac{k_n a_1}{a} J_{m+1} \left(\frac{k_n a_1}{a} \right) = m(1+\mu) J_m \left(\frac{k_n a_1}{a} \right), \tag{41}$$

from which $k_n (n = 1, 2, 3, \cdots)$ are determined. The ratio k_n/a is regarded as the radial wavenumber with increasing radial nodes with n. For numerical construction, we approximate $\hat{\phi}_1$ and $\hat{\phi}_2$ by a finite number N of the terms

$$\hat{\phi}_j \approx \hat{\phi}_j^{(N)} = \sum_{n=1}^{N} c_{jn} \hat{\phi}_{jn}, \ (j = 1, 2) \text{ for some } N \geq 1, \tag{42}$$

which is expected to approach the desired solution as N is increased.

3.3. Single-mode approximation for small values $\Omega^2 a/g$

First, we look into the axisymmetric instability ($m = 0$). Substituting $m = 0$ into (41) shows that k_n's are the zeros of $J_1(k_n a_1/a)$. To have an idea, we consider the case of a very low rotation rate ($\alpha = \Omega^2 a/g \ll 1$) and deduce an asymptotic expression of the eigenvalue ω, for a single trial function $\hat{\phi}_{1n}$ and $\hat{\phi}_{2n}$. By carrying out the integration (39) [27, 28] and then taking the partial derivatives $\partial\Phi/\partial c_{1n} = 0$ and $\partial\Phi/\partial c_{2n} = 0$, we obtain the eigenvalue ω, expanded in powers of α to $O(\alpha)$, as

$$\omega^2 \approx gA\frac{2k_n}{\sqrt{3}a_1}\tanh(k_n\hat{\delta}) + 2\Omega^2\left[1 + 2k_n\hat{\delta}\,\mathrm{csch}(2k_n\hat{\delta}) - \frac{1}{24}k_n^2A^2\ \mathrm{sech}^2(k_n\hat{\delta})\ -\frac{A}{36\hat{\delta}}\ \left(k_n\hat{\delta}\,\mathrm{sech}^2(k_n\hat{\delta}) + \tanh(k_n\hat{\delta})\right)\right], \tag{43}$$

where $\hat{\delta} = a_3/a_1$ is the aspect ratio. Given $g > 0$, we confirm the well-known result of RTI that, if the rotation is switched off ($\Omega = 0$), $A < 0$ leads to $\omega^2 < 0$, implying the instability. The form of (43) is different from the counterpart of [9]. The characteristic feature of (17) is that the parameter a appearing in (40) includes Ω, while, in the latter, a, being the radius of the circular cylinder, is fixed.

It should be noted that the last term in the bracket in (43) with coefficient $-A/36\hat{\delta}$ is intrinsic to the spheroidal geometry which is absent in the case of the circular cylinder of finite length. As mentioned in [9], (43) implies that the rotation act to relax the instability, that is, the negative first term is compensated for by the remaining terms which altogether have positive contribution. For RTI occurring when the Atwood number A is negative, the last term necessarily increases ω^2, signifying that, in the presence of rotation, the curvature of the container reinforces the stabilizing effect for RTI.

A care is exercised. In the critical parameter regime for RTI, the second term is comparable to the first, which may invalidate the expansion (43) in powers of the small parameter of α. Any definite conclusion cannot be drawn for the suppression of RTI. In the following subsection, a separate treatment is made when ω, rather than Ω, is small compared to $(a/g)^{1/2}$.

3.4. Single-mode approximation for small values of $\omega^2 a/g$

To convince ourselves the stabilization of RTI by the system rotation, we have to scrutinize the dispersion relation in the parameter regime where all the terms balance with each other, resulting in $\omega^2 \approx 0$.

We concentrate our attention on the regime near the stability threshold for which $\omega^2 a/g \ll 1$, with Ω left unrestricted. For $m = 0$, k_n is generated by $J_1(k_n a_1/a) = 0$. We impose $\alpha = \alpha_0 + a\omega^2\alpha_1/g + ...$, with α_0 and α_1 being constants to the determined

to leading order in $\omega^2 a/g$. For a single mode, the variational function is evaluated as

$$\Phi = \frac{(\rho_2-\rho_1)(1-\mu^2)\omega^2 a^2}{8g} J_0^2(k_n) \times \left\{ \left[\frac{1-A}{A} c_{1n} - \frac{1+A}{A} c_{2n} \right]^2 + \frac{1-A}{2A} \left[\frac{k_n^2}{12} + \frac{\delta k_n^2}{\alpha_0} \right] c_{1n}^2 - \frac{1+A}{2A} \left[\frac{k_n^2}{12} - \frac{\delta k_n^2}{\alpha_0} \right] c_{2n}^2 \right\}, \tag{44}$$

where $\delta = a_3/a$ with a defined by (16). This parameter should not be confused with the aspect ratio $\hat{\delta} = a_3/a_1$. The critical condition $\partial\Phi/\partial c_{1n} = 0$ and $\partial\Phi/\partial c_{2n} = 0$ gives rise to the dispersion relation, to leading order in α, as

$$\left\{ \frac{1-A}{A} + \frac{1}{2} \left[\frac{k_n^2}{12} + \frac{\delta k_n^2}{\alpha_0} \right] \right\} \left\{ \frac{1+A}{A} - \frac{1}{2} \left[\frac{k_n^2}{12} - \frac{\delta k_n^2}{\alpha_0} \right] \right\} - \frac{1-A^2}{A^2} = 0. \tag{45}$$

For the marginal state ($\omega = 0$), $\alpha = \alpha_0$, being a constant. We gain from (45) the critical value $\alpha_0 = \alpha_c$ and then the critical rotation rate Ω_c as

$$\frac{\Omega_c^2 a}{g} = \frac{6\delta}{A} \left(1 - \frac{k_n^2}{48} \right)^{-1} \left[\left\{ 1 - \frac{k_n^2 A^2}{12} \left(1 - \frac{k_n^2}{48} \right) \right\}^{\frac{1}{2}} - 1 \right]. \tag{46}$$

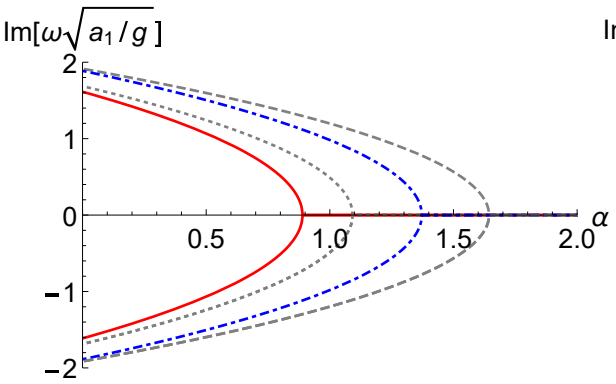

Figure 3. Comparison of the growth rate between oblate spheroids (43) and circular cylinders of finite length [9]. The oblate spheroid: $(a_1, a_3) = (4, 1)$ (solid line) and $(a_1, a_3) = (2, 1)$ (dot-dashed line). The circular cylinder of radius a_1 and length $2a_3$: $(a_1, a_3) = (4, 1)$ (dotted line) and $(a_1, a_3) = (2, 1)$ (dashed line). The Atwood number $A = -1$ for both cases. The horizontal axis is $\alpha = \Omega^2 a_1/g$ and the vertical axis is the imaginary part of $\omega\sqrt{a_1/g}$.

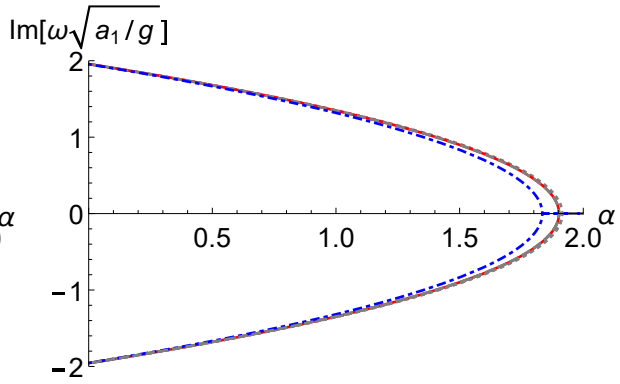

Figure 4. The same as Figure 3 but for prolate spheroids: $(a_1, a_3) = (1, 4)$ (solid line) and $(a_1, a_3) = (1, 1)$ (dot-dashed line). The circular cylinder of radius a_1 and length $2a_3$: $(a_1, a_3) = (1, 4)$ (dotted line) and $(a_1, a_3) = (1, 1)$ (dashed line).

Again we note that the parameter a includes the critical rotation rate Ω_c, as is seen from (17) in the case of small rotation rate Ω. The parameter k_n that counts complexity of the nodal structure of the perturbation increases monotonically with n, and, as a consequence, Ω_c^2 decreases with n. The critical rotation rate defined by (46) takes the maximum value for $n = 1$. This is the desired critical rotation rate.

Here we use the exact representation (16) for a and solve (46) numerically to get the critical rotation rate Ω_c. Figures 3 and Figure 4 show variation, with the aspect ratio $\hat{\delta} = a_3/a_1$, of the appropriately normalized growth rate $\mathrm{Im}[\omega]$ as a function of $\alpha = \Omega^2 a_1/g$ for oblate ($\hat{\delta} < 1$) and prolate ($\hat{\delta} > 1$) spheroids, respectively. The Atwood number $A = -1$ for both cases.

The aspect ratio $\hat{\delta}$ is a crucial parameter for the stability. The critical rotation rate Ω_{sp} for stability increases with $\hat{\delta}$. Larger rotation rate is required for being stabilized as the spheroid is elongated. In the limit of a thin circular plate ($\hat{\delta} \to 0$), the confined rotating flow is stable for any value of the rotation rate Ω. In order to compare of spheroids with finite circular cylinders of radius a_1 and length $2a_3$, with given aspect ratio a_3/a_1, we include the growth rate for the circular cylinder as well. In Figure 3 for the oblate spheroid, we draw the graphs for $(a_1, a_3) = (4, 1)$ (solid line), $(a_1, a_3) = (2, 1)$ (dot-dashed line), along with those for the circular cylinder of $(a_1, a_3) = (4, 1)$ (dotted line) and $(a_1, a_3) = (2, 1)$ (dashed line). In Figure 4 for an prolate spheroid, $(a_1, a_3) = (1, 4)$ (solid line) and $(a_1, a_3) = (1, 1)$ (dot-dashed line), along with $(a_1, a_3) = (1, 4)$ (dotted line) and $(a_1, a_3) = (1, 1)$ (dashed line) for the circular cylinder. Comparing the circular cylinder of finite length with the same aspect ratio, the critical rotation rate Ω_{sp} for a spheroid is smaller than Ω_{cy} for the circular cylinder [9]. This comparison demonstrates that the suppression of RTI by the system rotation is enhanced by the effect of topography of the container. This effect becomes more pronounced for an oblate spheroid than for a prolate spheroid, as is observed by comparing Figure 3 with Figure 4.

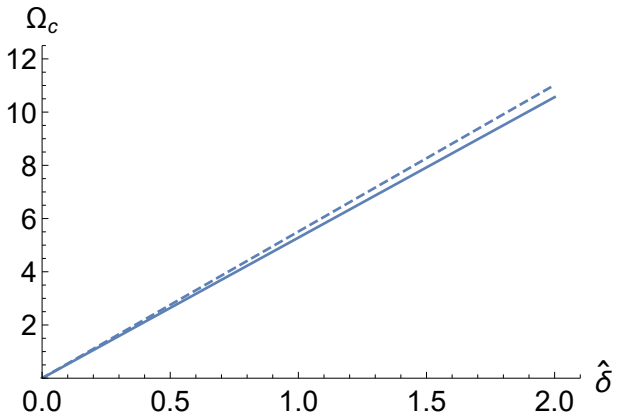

Figure 5. The critical rotation rate Ω_c against the aspect ratio $\hat{\delta} = a_3/a_1$ calculated from (46) with $n = 1$. The solid line is for the spheroid and the dashed line is for the finite circular cylinder. The oblate spheroid is corresponds to the range $0 \le \hat{\delta} < 1.0$ and the prolate is the range $1.0 < \hat{\delta}$. The sphere is achieved when $\hat{\delta} = 1$. The critical rotation rate Ω_c increases with $\hat{\delta}$.

A rough estimate of the critical rotation rate can be made with ease. Selecting

$n = 1$ gives $k_1 \approx 3.83(a/a_1)$ for the first zero $k \approx 3.83$ of $J_1(k)$ [27]. Because k_n/a is the radial wavenumber associated with the n-th radial mode, the corresponding radial wavelength is $\lambda = 2\pi a/k_1 = 2\pi a_1/3.83$ which is the same as the critical wavelength derived for the circular cylinder [9]. For the aspect ratio $\hat{\delta} = a_3/a_1 = 1/4$, we get the critical rotation rate $\Omega_{sp} = 1.32029$ for the oblate spheroid and $\Omega_{cy} = 1.78177$ for the finite cylinder. For the aspect ratio $\hat{\delta} = 2$, the critical rotation rate is $\Omega_{sp} = 10.5623$ for the prolate spheroid and $\Omega_{cy} = 11.02$ for the circular cylinder. For the aspect ratio $\hat{\delta} = 4$, the critical rotation rate is $\Omega_{sp} = 14.2542$ for the prolate spheroid with its cylindrical counterpart $\Omega_{cy} = 22.0401$. For fixing $n = 1$, the variation of the critical rotation rate Ω_c with the aspect ratio $\hat{\delta}$ is displayed in Figure 5. The solid line is Ω_{sp} for the spheroid and the dashed line is Ω_{cy} for the circular cylinder. The spherical symmetrical container ($\hat{\delta} = 1$) is included. We observe from Figure 5 that Ω_{sp} is always smaller than Ω_{cy}. Larger angular velocity of the system rotation is necessary for suppressing the instability as the spheroid is elongated.

We make an attempt at interpreting this dependence of Ω_{sp} on $\hat{\delta}$ on the ground of the gyroscopic analogy expounded in section 2. The moment I_1 and I_3 of the inertia reflect the shape of the spheroidal container. In view of (9), $I_1 < I_3$ for an oblate spheroid ($a_1 > a_3$), while $I_1 > I_3$ for an prolate spheroid ($a_1 < a_3$). The stability criterion (12) for the sleeping top dictates that, given σ_{30} and I_3, larger value of ω_{30}^2 is required for stability of the sleeping state for the prolate spheroid. This is consistent with our intuition and accounts for the above results of RTI for the discontinuous density distribution, or, the two-layer fluid. In this analogy, the gyroscopic term measured by ω_{30} corresponds to the Coriolis term parameterized by f. RTI of the two-layer flow in a spheroid is suppressed by the Coriolis force in the same way as as the sleeping top is stabilized by the gyroscopic term.

4. Conclusions and discussions

Unstably stratified flow with the Brunt-Väisälä frequency $N^2 < 0$ are gravitationally unstable. The Rayleigh-Taylor instability (RTI) is regarded as a special case. By rotating the system as a whole, the configuration of the unstably stratified state is maintained without being overturned, if the rotation rate is sufficiently large. So is the state of RTI in which a heavy fluid layer lies on top of a light fluid layer. The paper has shed light on the stabilizing mechanism of the system rotation by way of the analogy with motion of the Lagrange top, a heavy symmetrical rigid body, with a fixed point, undergoing the gravity force. The state of the sleeping top is likened to the unstable stratified flow.

The analogy with the Lagrange top becomes formally complete for the flow confined in a spheroid with the symmetric axis oriented in the vertical direction. The sleeping top is stable if the angular velocity about the symmetric axis is greater than the critical value as given by (12). A close look at (12) tells that larger angular velocity about the symmetric axis is necessary for a more elongated spheroid to be stabilized. A small

angular velocity is sufficient for an oblate spheroid, close to a circular plate, to be stabilized. With this background, we have examined the linear stability of a rotating flow confined in the lower-half of a spheroid covered by a rigid lid placed on the equatorial plane. A heavier fluid layer is sustained above a light fluid layer by rotating the system as a whole with its angular velocity greater than a critical value. The shape of the interface at the static state is a hyperboloid representing the isobaric surface. The form of the parameter a (16) makes distinction from the case of a circular cylinder of finite length [8, 9]. A higher rotation rate is required for stabilizing the two-layer rotating flow confined in a more elongated spheroid. Crudely speaking, the critical rotation rate increases linearly in the aspect ratio a_3/a_1. The qualitative feature is comprehensible by appealing to the analogy with the motion of the Lagrange top.

We have taken advantage of the variational formulation for calculating the dispersion relation [26, 8, 9]. This method provides an efficient way for calculating the dispersion relation and the critical rotation rate without entering into the detail of the flow field.

This study invites several questions. Some analogies with meteorological problems are worth pursuing [12]. We have ignored the viscosity and the heat conductivity. Thomson-Tait-Chetayev's theorem states that, for a system with an unstable potential, a state stabilized by gyroscopic forces goes unstable after the addition of arbitrary dissipation [30, 31]. In order to make clear the practical bearing of the stabilizing mechanism of rotation, we are requested to examine the effect of the viscosity and other dissipative mechanism. The motion of a free surface inside a spheroid is considered as the liquid sloshing, which finds application in rocketry [29]. This problem is approached by removing the solid lid placed on the equatorial plane. The effect of tilting the symmetric axis from the vertical direction may bring a dramatic effect as is inferred from rich behavior of the motion of a heavy rigid body. A rotating stratified fluid confined in an obliquely tilted spheroidal container draws an analogy with motion of a heavy symmetrical rigid body with the center of the gravity off the symmetric axis. Its stability is currently under investigation. An interest also arises as to the stability of a density interface on which the energy flux is produced as exemplified by the Landau-Darrieus instability for the flame front [32]. These and related effects call for independent investigation.

Acknowledgement

Y. F. is grateful to Boris A. Khesin who brought Dolzhansky's gyroscopic analogy to Y. F.'s attention. We also thank Geoffrey Vasil for invaluable comments. Y. F. was partially supported by a Grant-in-Aid for Scientific Research from the Japan Society for Promotion of Science (Grant No. 16K05476).

Reference

[1] Chandrasekhar S 1961 *Hydrodynamic and hydromagnetic stability* Oxford Univ. Press (Clarendon) London and New York

[2] Miles J W 1961 On the stability of heterogeneous shear flows *J. Fluid Mech.* **10** 496

[3] Fukumoto Y Sakuma H 2013 A unified view of topological invariants of barotropic and baroclinic fluids and their application to formal stability analysis of three-dimensional ideal gas flow *Procedia IUTAM* **7** "Topological Fluid Dynamics: Theory and Applications" 213

[4] Sakuma H, Fukumoto Y 2015 On formal stability of stratified shear flows *Publ. RIMS Kyoto Univ.* **51** 605

[5] Greenspan H P 1968 *The Theory of Rotating Fluids* (Cambridge University:Press New York)

[6] Gill A E 1982 *Atmosphere-Ocean Dynamic*s (Academic Press)

[7] Bühler O 2009 *Waves and Mean Flows* (Cambridge University Press)

[8] Baldwin K A, Scase M M, Hill R J A 2015 The inhibitation of the Rayleigh-Taylor instability by rotating *Nature Scientific Reports* 5:11706 DOI:10.1038/srep11706

[9] Scase M M, Baldwin K A, Hill R J A 2016 The rotating Rayleigh-Taylor instability arXiv:1603.00675v1

[10] Carnevale G F, Orlandi P, Zhou Ye, Kloosterziel R C 2002 Rotational suppression of Rayleigh-Taylor instability *J. Fluid Mech.* **457** 181

[11] Tao J J, Ye W H, Busse F H 2013 Nonlinear Rayleigh-Taylor instability of rotating inviscid fluid *Phys. Rev.* **87** 013001

[12] Dolzhansky F V 2012 *Fundamentals of geophysical hydrodynamics* transl. Khesin B A (Springer, Heidelberg)

[13] Miles J W, Ball F K 1963 On free-surface oscillations in a rotating paraboloid *J. Fluid Mech.* **17** 257

[14] Greenhill A G 1879 On the relation of a liquid ellipsoid about its mean axis *Proc. Cambridge Philos. Soc.***3** 233

[15] Poincaré H 1910 On the precession of deformable bodies *Bull. AStr.* **27** 321

[16] Vallis G K 2012 *Atmospheric and oceanic fluid dynamics* (Cambridge University Press, Cambridge, U.K.)

[17] Dolzhansky F V 2002 On the mechanical prototypes of the fundamental hydrodynamic invariants and slow manifolds *UFN* **175** 12

[18] Glukhovsky A B, Dolzhansky F V 1980 Three-mode geostrophical convection models of a rotating fluid *Izv. Academy of Sciences USSR, Ser. FAO*, **16** 5

[19] Dolzhansky F V, Ponomarev V M 2002 The simplest slow manifolds of barotropic and baroclinic motions of a rotating fluid *Izv. RAN Ser. FAO* **38** 277

[20] Gledzer A E 2003 On slow motions in the reduced equations of a stratified fluid in a Coriolis force field *Izv. RAN Ser. FAO* **6** 662

[21] Holm D D 1986 Gyroscopic analog for collective motion of a stratified fluid *J. Math. Anal. Appl.* **117** 57

[22] Davey M K, Whitehead J A Jr. 1981 Rotating Rayleigh-Taylor instability as a model of sinking events in the ocean *Geophys. Astrophys. Fluid Dynamics* **17** 237

[23] Arnold V I 1978 *Mathematical Methods of Classical Mechanics* (Springer, Berlin)

[24] Fukumoto Y 1997 Stationary configurations of a vortex filament in background flows *Proc. R. Soc. Lond. A* **453** 1205

[25] Hart R W 1981 Generalized scalar potentials for linearized three-dimensional flows with vorticity *Phys. Fluids* **24** 1418

[26] Miles J W 1964 Free-surface oscillations in a slowly rotating fluid *J. Fluid Mech.* **18** 187

[27] Watson G N 1945 *A Treatise on the Theory of Bessel Functions* (Cambridge University Press NewYork)

[28] Erdélyi A, Magnus W, Oberhettinger F, Tricomi F G 1954 *Tables of Integral Transformations* vol.

II (New York, McGraw-Hill Book Co)
[29] Bauer H F, Eidel W 1989 Liquid oscillations in a prolate spheroidal container *Ingenieur-Archiv* **56** 371
[30] Merkin D R 1996 *Introduction to the Theory of Stability* trans. Smirnov A L, Afagh F F (Springer, Heidelberg)
[31] Paerhati A, Fukumoto Y 2013 An example exempted from Thomson-Tait-Chetayev's Theorem *J. Phys. Soc. Jpn.* **82** 043002
[32] Abarzhi S I, Fukumoto Y, Kadanoff L P 2015 Stability of a hydrodynamic discontinuity *Physica Scri.* **90** 018002

List of MI Preprint Series, Kyushu University

The Global COE Program
Math-for-Industry Education & Research Hub

MI

MI2008-1 Takahiro ITO, Shuichi INOKUCHI & Yoshihiro MIZOGUCHI
Abstract collision systems simulated by cellular automata

MI2008-2 Eiji ONODERA
The intial value problem for a third-order dispersive flow into compact almost Hermitian manifolds

MI2008-3 Hiroaki KIDO
On isosceles sets in the 4-dimensional Euclidean space

MI2008-4 Hirofumi NOTSU
Numerical computations of cavity flow problems by a pressure stabilized characteristic-curve finite element scheme

MI2008-5 Yoshiyasu OZEKI
Torsion points of abelian varieties with values in nfinite extensions over a p-adic field

MI2008-6 Yoshiyuki TOMIYAMA
Lifting Galois representations over arbitrary number fields

MI2008-7 Takehiro HIROTSU & Setsuo TANIGUCHI
The random walk model revisited

MI2008-8 Silvia GANDY, Masaaki KANNO, Hirokazu ANAI & Kazuhiro YOKOYAMA
Optimizing a particular real root of a polynomial by a special cylindrical algebraic decomposition

MI2008-9 Kazufumi KIMOTO, Sho MATSUMOTO & Masato WAKAYAMA
Alpha-determinant cyclic modules and Jacobi polynomials

MI2008-10 Sangyeol LEE & Hiroki MASUDA
Jarque-Bera Normality Test for the Driving Lévy Process of a Discretely Observed Univariate SDE

MI2008-11 Hiroyuki CHIHARA & Eiji ONODERA
A third order dispersive flow for closed curves into almost Hermitian manifolds

MI2008-12 Takehiko KINOSHITA, Kouji HASHIMOTO and Mitsuhiro T. NAKAO
On the L^2 a priori error estimates to the finite element solution of elliptic problems with singular adjoint operator

MI2008-13 Jacques FARAUT and Masato WAKAYAMA
Hermitian symmetric spaces of tube type and multivariate Meixner-Pollaczek polynomials

MI2008-14 Takashi NAKAMURA
Riemann zeta-values, Euler polynomials and the best constant of Sobolev inequality

MI2008-15 Takashi NAKAMURA
Some topics related to Hurwitz-Lerch zeta functions

MI2009-1 Yasuhide FUKUMOTO
Global time evolution of viscous vortex rings

MI2009-2 Hidetoshi MATSUI & Sadanori KONISHI
Regularized functional regression modeling for functional response and predictors

MI2009-3 Hidetoshi MATSUI & Sadanori KONISHI
Variable selection for functional regression model via the L_1 regularization

MI2009-4 Shuichi KAWANO & Sadanori KONISHI
Nonlinear logistic discrimination via regularized Gaussian basis expansions

MI2009-5 Toshiro HIRANOUCHI & Yuichiro TAGUCHII
Flat modules and Groebner bases over truncated discrete valuation rings

MI2009-6 Kenji KAJIWARA & Yasuhiro OHTA
Bilinearization and Casorati determinant solutions to non-autonomous 1+1 dimensional discrete soliton equations

MI2009-7 Yoshiyuki KAGEI
Asymptotic behavior of solutions of the compressible Navier-Stokes equation around the plane Couette flow

MI2009-8 Shohei TATEISHI, Hidetoshi MATSUI & Sadanori KONISHI
Nonlinear regression modeling via the lasso-type regularization

MI2009-9 Takeshi TAKAISHI & Masato KIMURA
Phase field model for mode III crack growth in two dimensional elasticity

MI2009-10 Shingo SAITO
Generalisation of Mack's formula for claims reserving with arbitrary exponents for the variance assumption

MI2009-11 Kenji KAJIWARA, Masanobu KANEKO, Atsushi NOBE & Teruhisa TSUDA
Ultradiscretization of a solvable two-dimensional chaotic map associated with the Hesse cubic curve

MI2009-12 Tetsu MASUDA
Hypergeometric τ-functions of the q-Painlevé system of type $E_8^{(1)}$

MI2009-13 Hidenao IWANE, Hitoshi YANAMI, Hirokazu ANAI & Kazuhiro YOKOYAMA
A Practical Implementation of a Symbolic-Numeric Cylindrical Algebraic Decomposition for Quantifier Elimination

MI2009-14 Yasunori MAEKAWA
On Gaussian decay estimates of solutions to some linear elliptic equations and its applications

MI2009-15 Yuya ISHIHARA & Yoshiyuki KAGEI
Large time behavior of the semigroup on L^p spaces associated with the linearized compressible Navier-Stokes equation in a cylindrical domain

MI2009-16 Chikashi ARITA, Atsuo KUNIBA, Kazumitsu SAKAI & Tsuyoshi SAWABE
Spectrum in multi-species asymmetric simple exclusion process on a ring

MI2009-17 Masato WAKAYAMA & Keitaro YAMAMOTO
Non-linear algebraic differential equations satisfied by certain family of elliptic functions

MI2009-18 Me Me NAING & Yasuhide FUKUMOTO
Local Instability of an Elliptical Flow Subjected to a Coriolis Force

MI2009-19 Mitsunori KAYANO & Sadanori KONISHI
Sparse functional principal component analysis via regularized basis expansions and its application

MI2009-20 Shuichi KAWANO & Sadanori KONISHI
Semi-supervised logistic discrimination via regularized Gaussian basis expansions

MI2009-21 Hiroshi YOSHIDA, Yoshihiro MIWA & Masanobu KANEKO
Elliptic curves and Fibonacci numbers arising from Lindenmayer system with symbolic computations

MI2009-22 Eiji ONODERA
A remark on the global existence of a third order dispersive flow into locally Hermitian symmetric spaces

MI2009-23 Stjepan LUGOMER & Yasuhide FUKUMOTO
Generation of ribbons, helicoids and complex scherk surface in laser-matter Interactions

MI2009-24 Yu KAWAKAMI
Recent progress in value distribution of the hyperbolic Gauss map

MI2009-25 Takehiko KINOSHITA & Mitsuhiro T. NAKAO
On very accurate enclosure of the optimal constant in the a priori error estimates for H_0^2-projection

MI2009-26 Manabu YOSHIDA
Ramification of local fields and Fontaine's property (Pm)

MI2009-27 Yu KAWAKAMI
Value distribution of the hyperbolic Gauss maps for flat fronts in hyperbolic three-space

MI2009-28 Masahisa TABATA
Numerical simulation of fluid movement in an hourglass by an energy-stable finite element scheme

MI2009-29 Yoshiyuki KAGEI & Yasunori MAEKAWA
Asymptotic behaviors of solutions to evolution equations in the presence of translation and scaling invariance

MI2009-30 Yoshiyuki KAGEI & Yasunori MAEKAWA
On asymptotic behaviors of solutions to parabolic systems modelling chemotaxis

MI2009-31 Masato WAKAYAMA & Yoshinori YAMASAKI
Hecke's zeros and higher depth determinants

MI2009-32 Olivier PIRONNEAU & Masahisa TABATA
Stability and convergence of a Galerkin-characteristics finite element scheme of lumped mass type

MI2009-33 Chikashi ARITA
Queueing process with excluded-volume effect

MI2009-34 Kenji KAJIWARA, Nobutaka NAKAZONO & Teruhisa TSUDA
Projective reduction of the discrete Painlevé system of type$(A_2 + A_1)^{(1)}$

MI2009-35 Yosuke MIZUYAMA, Takamasa SHINDE, Masahisa TABATA & Daisuke TAGAMI
Finite element computation for scattering problems of micro-hologram using DtN map

MI2009-36 Reiichiro KAWAI & Hiroki MASUDA
Exact simulation of finite variation tempered stable Ornstein-Uhlenbeck processes

MI2009-37 Hiroki MASUDA
On statistical aspects in calibrating a geometric skewed stable asset price model

MI2010-1 Hiroki MASUDA
Approximate self-weighted LAD estimation of discretely observed ergodic Ornstein-Uhlenbeck processes

MI2010-2 Reiichiro KAWAI & Hiroki MASUDA
Infinite variation tempered stable Ornstein-Uhlenbeck processes with discrete observations

MI2010-3 Kei HIROSE, Shuichi KAWANO, Daisuke MIIKE & Sadanori KONISHI
Hyper-parameter selection in Bayesian structural equation models

MI2010-4 Nobuyuki IKEDA & Setsuo TANIGUCHI
The Itô-Nisio theorem, quadratic Wiener functionals, and 1-solitons

MI2010-5 Shohei TATEISHI & Sadanori KONISHI
Nonlinear regression modeling and detecting change point via the relevance vector machine

MI2010-6 Shuichi KAWANO, Toshihiro MISUMI & Sadanori KONISHI
Semi-supervised logistic discrimination via graph-based regularization

MI2010-7 Teruhisa TSUDA
UC hierarchy and monodromy preserving deformation

MI2010-8 Takahiro ITO
Abstract collision systems on groups

MI2010-9 Hiroshi YOSHIDA, Kinji KIMURA, Naoki YOSHIDA, Junko TANAKA & Yoshihiro MIWA
An algebraic approach to underdetermined experiments

MI2010-10 Kei HIROSE & Sadanori KONISHI
Variable selection via the grouped weighted lasso for factor analysis models

MI2010-11 Katsusuke NABESHIMA & Hiroshi YOSHIDA
Derivation of specific conditions with Comprehensive Groebner Systems

MI2010-12 Yoshiyuki KAGEI, Yu NAGAFUCHI & Takeshi SUDOU
Decay estimates on solutions of the linearized compressible Navier-Stokes equation around a Poiseuille type flow

MI2010-13 Reiichiro KAWAI & Hiroki MASUDA
On simulation of tempered stable random variates

MI2010-14 Yoshiyasu OZEKI
Non-existence of certain Galois representations with a uniform tame inertia weight

MI2010-15 Me Me NAING & Yasuhide FUKUMOTO
Local Instability of a Rotating Flow Driven by Precession of Arbitrary Frequency

MI2010-16 Yu KAWAKAMI & Daisuke NAKAJO
The value distribution of the Gauss map of improper affine spheres

MI2010-17 Kazunori YASUTAKE
On the classification of rank 2 almost Fano bundles on projective space

MI2010-18 Toshimitsu TAKAESU
Scaling limits for the system of semi-relativistic particles coupled to a scalar bose field

MI2010-19 Reiichiro KAWAI & Hiroki MASUDA
Local asymptotic normality for normal inverse Gaussian Lévy processes with high-frequency sampling

MI2010-20 Yasuhide FUKUMOTO, Makoto HIROTA & Youichi MIE
Lagrangian approach to weakly nonlinear stability of an elliptical flow

MI2010-21 Hiroki MASUDA
Approximate quadratic estimating function for discretely observed Lévy driven SDEs with application to a noise normality test

MI2010-22 Toshimitsu TAKAESU
A Generalized Scaling Limit and its Application to the Semi-Relativistic Particles System Coupled to a Bose Field with Removing Ultraviolet Cutoffs

MI2010-23 Takahiro ITO, Mitsuhiko FUJIO, Shuichi INOKUCHI & Yoshihiro MIZOGUCHI
Composition, union and division of cellular automata on groups

MI2010-24 Toshimitsu TAKAESU
A Hardy's Uncertainty Principle Lemma in Weak Commutation Relations of Heisenberg-Lie Algebra

MI2010-25 Toshimitsu TAKAESU
On the Essential Self-Adjointness of Anti-Commutative Operators

MI2010-26 Reiichiro KAWAI & Hiroki MASUDA
On the local asymptotic behavior of the likelihood function for Meixner Lévy processes under high-frequency sampling

MI2010-27 Chikashi ARITA & Daichi YANAGISAWA
Exclusive Queueing Process with Discrete Time

MI2010-28 Jun-ichi INOGUCHI, Kenji KAJIWARA, Nozomu MATSUURA & Yasuhiro OHTA
Motion and Bäcklund transformations of discrete plane curves

MI2010-29 Takanori YASUDA, Masaya YASUDA, Takeshi SHIMOYAMA & Jun KOGURE
On the Number of the Pairing-friendly Curves

MI2010-30 Chikashi ARITA & Kohei MOTEGI
Spin-spin correlation functions of the q-VBS state of an integer spin model

MI2010-31 Shohei TATEISHI & Sadanori KONISHI
Nonlinear regression modeling and spike detection via Gaussian basis expansions

MI2010-32 Nobutaka NAKAZONO
Hypergeometric τ functions of the q-Painlevé systems of type $(A_2 + A_1)^{(1)}$

MI2010-33 Yoshiyuki KAGEI
Global existence of solutions to the compressible Navier-Stokes equation around parallel flows

MI2010-34 Nobushige KUROKAWA, Masato WAKAYAMA & Yoshinori YAMASAKI
Milnor-Selberg zeta functions and zeta regularizations

MI2010-35 Kissani PERERA & Yoshihiro MIZOGUCHI
Laplacian energy of directed graphs and minimizing maximum outdegree algorithms

MI2010-36 Takanori YASUDA
CAP representations of inner forms of $Sp(4)$ with respect to Klingen parabolic subgroup

MI2010-37 Chikashi ARITA & Andreas SCHADSCHNEIDER
Dynamical analysis of the exclusive queueing process

MI2011-1 Yasuhide FUKUMOTO& Alexander B. SAMOKHIN
Singular electromagnetic modes in an anisotropic medium

MI2011-2 Hiroki KONDO, Shingo SAITO & Setsuo TANIGUCHI
Asymptotic tail dependence of the normal copula

MI2011-3 Takehiro HIROTSU, Hiroki KONDO, Shingo SAITO, Takuya SATO, Tatsushi TANAKA & Setsuo TANIGUCHI
Anderson-Darling test and the Malliavin calculus

MI2011-4 Hiroshi INOUE, Shohei TATEISHI & Sadanori KONISHI
Nonlinear regression modeling via Compressed Sensing

MI2011-5 Hiroshi INOUE
Implications in Compressed Sensing and the Restricted Isometry Property

MI2011-6 Daeju KIM & Sadanori KONISHI
Predictive information criterion for nonlinear regression model based on basis expansion methods

MI2011-7 Shohei TATEISHI, Chiaki KINJYO & Sadanori KONISHI
Group variable selection via relevance vector machine

MI2011-8 Jan BREZINA & Yoshiyuki KAGEI
Decay properties of solutions to the linearized compressible Navier-Stokes equation around time-periodic parallel flow
Group variable selection via relevance vector machine

MI2011-9 Chikashi ARITA, Arvind AYYER, Kirone MALLICK & Sylvain PROLHAC
Recursive structures in the multispecies TASEP

MI2011-10 Kazunori YASUTAKE
On projective space bundle with nef normalized tautological line bundle

MI2011-11 Hisashi ANDO, Mike HAY, Kenji KAJIWARA & Tetsu MASUDA
An explicit formula for the discrete power function associated with circle patterns of Schramm type

MI2011-12 Yoshiyuki KAGEI
Asymptotic behavior of solutions to the compressible Navier-Stokes equation around a parallel flow

MI2011-13 Vladimír CHALUPECKÝ & Adrian MUNTEAN
Semi-discrete finite difference multiscale scheme for a concrete corrosion model: approximation estimates and convergence

MI2011-14 Jun-ichi INOGUCHI, Kenji KAJIWARA, Nozomu MATSUURA & Yasuhiro OHTA
Explicit solutions to the semi-discrete modified KdV equation and motion of discrete plane curves

MI2011-15 Hiroshi INOUE
A generalization of restricted isometry property and applications to compressed sensing

MI2011-16 Yu KAWAKAMI
A ramification theorem for the ratio of canonical forms of flat surfaces in hyperbolic three-space

MI2011-17 Naoyuki KAMIYAMA
Matroid intersection with priority constraints

MI2012-1 Kazufumi KIMOTO & Masato WAKAYAMA
Spectrum of non-commutative harmonic oscillators and residual modular forms

MI2012-2 Hiroki MASUDA
Mighty convergence of the Gaussian quasi-likelihood random fields for ergodic Levy driven SDE observed at high frequency

MI2012-3 Hiroshi INOUE
A Weak RIP of theory of compressed sensing and LASSO

MI2012-4 Yasuhide FUKUMOTO & Youich MIE
Hamiltonian bifurcation theory for a rotating flow subject to elliptic straining field

MI2012-5 Yu KAWAKAMI
On the maximal number of exceptional values of Gauss maps for various classes of surfaces

MI2012-6 Marcio GAMEIRO, Yasuaki HIRAOKA, Shunsuke IZUMI, Miroslav KRAMAR, Konstantin MISCHAIKOW & Vidit NANDA
Topological Measurement of Protein Compressibility via Persistence Diagrams

MI2012-7 Nobutaka NAKAZONO & Seiji NISHIOKA
Solutions to a q-analog of Painlevé III equation of type $D_7^{(1)}$

MI2012-8 Naoyuki KAMIYAMA
A new approach to the Pareto stable matching problem

MI2012-9 Jan BREZINA & Yoshiyuki KAGEI
Spectral properties of the linearized compressible Navier-Stokes equation around time-periodic parallel flow

MI2012-10 Jan BREZINA
Asymptotic behavior of solutions to the compressible Navier-Stokes equation around a time-periodic parallel flow

MI2012-11 Daeju KIM, Shuichi KAWANO & Yoshiyuki NINOMIYA
Adaptive basis expansion via the extended fused lasso

MI2012-12 Masato WAKAYAMA
On simplicity of the lowest eigenvalue of non-commutative harmonic oscillators

MI2012-13 Masatoshi OKITA
On the convergence rates for the compressible
Navier- Stokes equations with potential force

MI2013-1 Abuduwaili PAERHATI & Yasuhide FUKUMOTO
A Counter-example to Thomson-Tait-Chetayev's Theorem

MI2013-2 Yasuhide FUKUMOTO & Hirofumi SAKUMA
A unified view of topological invariants of barotropic and baroclinic fluids and their application to formal stability analysis of three-dimensional ideal gas flows

MI2013-3 Hiroki MASUDA
Asymptotics for functionals of self-normalized residuals of discretely observed stochastic processes

MI2013-4 Naoyuki KAMIYAMA
On Counting Output Patterns of Logic Circuits

MI2013-5 Hiroshi INOUE
RIPless Theory for Compressed Sensing

MI2013-6 Hiroshi INOUE
Improved bounds on Restricted isometry for compressed sensing

MI2013-7 Hidetoshi MATSUI
Variable and boundary selection for functional data via multiclass logistic regression modeling

MI2013-8 Hidetoshi MATSUI
Variable selection for varying coefficient models with the sparse regularization

MI2013-9 Naoyuki KAMIYAMA
Packing Arborescences in Acyclic Temporal Networks

MI2013-10 Masato WAKAYAMA
Equivalence between the eigenvalue problem of non-commutative harmonic oscillators and existence of holomorphic solutions of Heun's differential equations, eigenstates degeneration, and Rabi's model

MI2013-11 Masatoshi OKITA
Optimal decay rate for strong solutions in critical spaces to the compressible Navier-Stokes equations

MI2013-12 Shuichi KAWANO, Ibuki HOSHINA, Kazuki MATSUDA & Sadanori KONISHI
Predictive model selection criteria for Bayesian lasso

MI2013-13 Hayato CHIBA
The First Painleve Equation on the Weighted Projective Space

MI2013-14 Hidetoshi MATSUI
Variable selection for functional linear models with functional predictors and a functional response

MI2013-15 Naoyuki KAMIYAMA
The Fault-Tolerant Facility Location Problem with Submodular Penalties

MI2013-16 Hidetoshi MATSUI
Selection of classification boundaries using the logistic regression

MI2014-1 Naoyuki KAMIYAMA
Popular Matchings under Matroid Constraints

MI2014-2 Yasuhide FUKUMOTO & Youichi MIE
Lagrangian approach to weakly nonlinear interaction of Kelvin waves and a symmetry-breaking bifurcation of a rotating flow

MI2014-3 Reika AOYAMA
Decay estimates on solutions of the linearized compressible Navier-Stokes equation around a Parallel flow in a cylindrical domain

MI2014-4 Naoyuki KAMIYAMA
The Popular Condensation Problem under Matroid Constraints

MI2014-5 Yoshiyuki KAGEI & Kazuyuki TSUDA
Existence and stability of time periodic solution to the compressible Navier-Stokes equation for time periodic external force with symmetry

MI2014-6 This paper was withdrawn by the authors.

MI2014-7 Masatoshi OKITA
On decay estimate of strong solutions in critical spaces for the compressible Navier-Stokes equations

MI2014-8 Rong ZOU & Yasuhide FUKUMOTO
Local stability analysis of azimuthal magnetorotational instability of ideal MHD flows

MI2014-9 Yoshiyuki KAGEI & Naoki MAKIO
Spectral properties of the linearized semigroup of the compressible Navier-Stokes equation on a periodic layer

MI2014-10 Kazuyuki TSUDA
On the existence and stability of time periodic solution to the compressible Navier-Stokes equation on the whole space

MI2014-11 Yoshiyuki KAGEI & Takaaki NISHIDA
Instability of plane Poiseuille flow in viscous compressible gas

MI2014-12 Chien-Chung HUANG, Naonori KAKIMURA & Naoyuki KAMIYAMA
Exact and approximation algorithms for weighted matroid intersection

MI2014-13 Yusuke SHIMIZU
Moment convergence of regularized least-squares estimator for linear regression model

MI2015-1 Hidetoshi MATSUI & Yuta UMEZU
Sparse regularization for multivariate linear models for functional data

MI2015-2 Reika AOYAMA & Yoshiyuki KAGEI
Spectral properties of the semigroup for the linearized compressible Navier-Stokes equation around a parallel flow in a cylindrical domain

MI2015-3 Naoyuki KAMIYAMA
Stable Matchings with Ties, Master Preference Lists, and Matroid Constraints

MI2015-4 Reika AOYAMA & Yoshiyuki KAGEI
Large time behavior of solutions to the compressible Navier-Stokes equations around a parallel flow in a cylindrical domain

MI2015-5 Kazuyuki TSUDA
Existence and stability of time periodic solution to the compressible Navier-Stokes-Korteweg system on R^3

MI2015-6 Naoyuki KAMIYAMA
Popular Matchings with Ties and Matroid Constraints

MI2015-7 Shoichi EGUCHI & Hiroki MASUDA
Quasi-Bayesian model comparison for LAQ models

MI2015-8 Yoshiyuki KAGEI & Ryouta OOMACHI
Stability of time periodic solution of the Navier-Stokes equation on the half-space under oscillatory moving boundary condition

MI2016-1 Momonari KUDO
Analysis of an algorithm to compute the cohomology groups of coherent sheaves and its applications

MI2016-2 Yoshiyuki KAGEI & Masatoshi OKITA
Asymptotic profiles for the compressible Navier-Stokes equations on the whole space

MI2016-3 Shota ENOMOTO & Yoshiyuki KAGEI
Asymptotic behavior of the linearized semigroup at space-periodic stationary solution of the compressible Navier-Stokes equation

MI2016-4 Hiroki MASUDA
Non-Gaussian quasi-likelihood estimation of locally stable SDE

MI2016-5 Yoshiyuki KAGEI & Takaaki NISHIDA
On Chorin's method for stationary solutions of the Oberbeck-Boussinesq equation

MI2016-6 Hayato WAKI & Florin NAE
Boundary modeling in model-based calibration for automotive engines via the vertex representation of the convex hulls

MI2016-7 Kazuyuki TSUDA
Time periodic problem for the compressible Navier-Stokes equation on R^2 with antisymmetry

MI2016-8 Abulizi AIHAITI, Shota ENOMOTO & Yoshiyuki KAGEI
Large time behavior of solutions to the compressible Navier-Stokes equations in an infinite layer under slip boundary condition

MI2016-9 Fermín Franco MEDRANO, Yasuhide FUKUMOTO, Clara M. VELTE & Azur HODŽIĆ
Gas entrainment rate coefficient of an ideal momentum atomizing liquid jet

MI2016-10 Naoyuki KAMIYAMA, Akifumi KIRA, Hirokazu ANAI, Hidenao IWANE & Kotaro OHORI
Coalition Structure Generation with Subadditivity Constraints

MI2016-11 Akifumi KIRA, Hidenao IWANE, Hirokazu ANAI, Yutaka KIMURA & Katsuki FUJISAWA
An indirect search algorithm for disaster restoration with precedence and synchronization constraints

MI2016-12 Shota ENOMOTO
Large time behavior of the solutions around spatially periodic solution to the compressible Navier-Stokes equation

MI2016-13 Naoyuki KAMIYAMA
Popular Matchings with Two-Sided Preference Lists and Matroid Constraints

MI2016-14 Naoyuki KAMIYAMA
An Algorithm for the Evacuation Problem based on Parametric Submodular Function Minimization

MI2016-15 Naoyuki KAMIYAMA
A Note on Submodular Function Minimization with Covering Type Linear Constraints

MI2017-1 Yuki MIYACHI & Yasuhide FUKUMOTO
Gyroscopic Analogy of Coriolis Effect of Rotating Stratified Flows Confined in a Spheroid